THE ASTROPHYSICAL JOURNAL, 409:412–416, 1993 May 20

SPATIALLY RESOLVED SPECTRA OF THE UNIDENTIFIED INFRARED FEATURES AROUND HD 44179 (THE RED RECTANGLE)[1]

G. C. SLOAN[2]
Department of Physics and Astronomy, University of Wyoming
G. L. GRASDALEN
G-Star Enterprises, 286 South Pennsylvania, Denver, CO 80209
AND
PAUL D. LEVAN[3]
Phillips Laboratory, PL/GPOB, Hanscom AFB
Received 1992 September 8; accepted 1992 November 16

ABSTRACT

We have observed HD 44179 and the surrounding unidentified infrared (UIR) emission with a long-slit 10 μm spectrometer. By applying maximum entropy reconstruction methods to our images, we have found spatial variations in the spectra not apparent in previous work with beam sizes of several arcseconds diameter. We find that no UIR emission arises in the innermost regions of the source; instead, we observe only cool continuum emission. After its abrupt appearance 0".5 from the central source, the UIR emission decays steadily with distance, except for an enhancement in the intensity of the 11.3 μm feature $\sim$1".5 away from the central source. The intensity of the 7.7 μm feature drops more quickly with distance than the intensity of the 8.6 and 11.3 μm features, and the wavelength of peak intensity of this feature appears to shift from 7.9 μm near the central source to $\sim$7.4 μm further away. These observations indicate that we have detected the formation of the carriers of the UIR emission features and changes in their emission properties as they move outward. In particular, the behavior of the 8.6 and 11.3 μm features suggest the material is growing increasingly hydrogenated with distance. We suggest that all the unusual spectral properties of this sytem can be explained in terms of an accretion disk around a degenerate object.

Subject headings: infrared: interstellar: continuum — ISM: individual (Red Rectangle) — stars: individual (HD 44179)

1. INTRODUCTION

HD 44179 was detected as a bright infrared source in the Air Force Cambridge Research Laboratory's rocket sky survey (Walker & Price 1975). It has since become one of the most studied sources of the unidentified infrared (UIR) emission features. Cohen et al. (1975) associated the infrared source with the star HD 44179 and a nearly rectangular object extended $\sim$40" north/south on the red Palomar Sky Survey plates. The central star, which they classified as B9-A0 III, is embedded in a bipolar reflection nebula. We will refer to the central source as HD 44179 and the surrounding nebulosity as the Red Rectangle. Because of its unusual morphology, its carbon-rich nature, its Galactic latitude ($-12°$), and the lack of interstellar material in the region, Zuckerman et al. (1976) argue that the object is a proto–planetary nebula.

The UIR features were first detected by Gillett, Forrest, & Merrill (1973) in spectra of the planetary nebulae BD +30°3639 and NGC 7027. Merrill soon after observed these features in the Red Rectangle (Cohen et al. 1975). Since that time, several hypotheses have been introduced to explain the carriers of the features. Most invoke small particles which are briefly heated to 1000 K by the absorption of a UV photon and are sufficiently refractory to survive intact, an idea advanced by Sellgren (1984) to explain the near-infrared continuum she observed in reflection nebulae. For this reason, carbon has been the basis of all the models, an argument strongly supported by the correlation between C/O ratio and 7.7 μm flux discovered for several planetary nebulae by Cohen et al. (1986).

A widely accepted explanation of the UIR features is the polycyclic aromatic hydrocarbon (PAH) model, which suggests that the features arise from C—H and C—C bonds in large molecules consisting of hydrogenated aromatic rings (Allamandola, Tielens, & Barker 1985, 1989; Léger & Puget 1984; Léger, d'Hendecourt, & Défourneau 1989). Other models include hydrogenated amorphous carbon (HAC; Jones, Duley, & Williams 1990; Blanco, Bussoletti, & Colangeli 1988, and references therein) and quenched carbonaceous composites (QCC; Sakata et al. 1984, 1987, 1990).

HD 44179 is extended on the order of 1" in the near-infrared (Dainty et al. 1985; Leinert & Haas 1989). Geballe et al. (1989) have found the emission from the 3.3 μm UIR feature is detectable in a 5" beam centered 5" north of HD 44179. While the feature emission is 60 times weaker than in the central region, it is nevertheless clear that its shape differs, having a higher proportion of emission at 3.4 μm and other features not seen in the central region as well.

We chose to observe the Red Rectangle with a long-slit 10 μm spectrometer to extend these studies of the spatial nature of the UIR emission to features seen in the 10 μm band. Spatial variations in the nature of the UIR emission may allow us to distinguish between the different models of the carriers of the UIR emission. In Grasdalen, Sloan, & LeVan (1992, hereafter Paper I), we published preliminary results of our observations. By fitting a spatial profile to the object at each wavelength in

[1] Contribution 137 of the Wyoming Infrared Observatory.
[2] Postal address: Phillips Laboratory, PL/GPOB, Hanscom AFB, MA 01731.
[3] Postal address: Phillips Laboratory, PL/VTRP, Kirtland, AFB, NM 87117.

our spectral images, we showed that the object was spatially extended at the wavelengths of all four UIR features detected between 7 and 14 μm. To gain a better understanding of the behavior of the UIR features with position in our images, we have chosen to apply maximum entropy techniques to our data. Here, we present the results of our maximum entropy reconstructions.

2. OBSERVATIONS AND DATA REDUCTION

We observed the Red Rectangle with the Air Force Geophysics Laboratory 10 μm Array Detector Spectrometer (GLADYS; LeVan 1990) mounted at the Cassegrain focus of the 2.3 m reflecting telescope of the Wyoming Infrared Observatory (WIRO). We made our observations by reading a 10×62 portion of the Si:Ga array; each of the 10 rows spans 0.″88 of the sky along the slit. We performed background subtraction using the three-beam chop method described by Landau, Grasdalen, & Sloan (1992), chopping at 1.5 Hz with a throw of 23″ north and south of the object. The slit was oriented in the same direction as the chop.

Observations taken on 1991 February 10 consisted of 40 images of the Red Rectangle and 40 images of α Tau, which we used as a spectroscopic and point source reference. The data were taken in two sets, with the Red Rectangle observations sandwiched between observations of our standard in each. In the first set each image of the Red Rectangle consisted of 240 chops, while each α Tau image represents 80 chops. We improved the focus and increased the integration time for the second set of data, collecting 320 chops in each Red Rectangle image and 160 in each α Tau image.

The images were flat-fielded as described in Paper I. Before extracting spectra, we used maximum entropy techniques to reconstruct our images, using a modification of the MEMSYS algorithm of Gull & Skilling (1984, 1989). In our study of α Ori (Sloan, Grasdalen, & LeVan 1993, hereafter Paper II), we optimized our maximum entropy algorithm by carefully studying its effects on observations of point sources, simulations of extended sources, and the α Ori images themselves. The resultant algorithm is described in Paper II. We used our observations of α Tau to determine the behavior of the point spread function (PSF) with wavelength.

We reconstructed each of the 40 Red Rectangle images separately. We originally tried to improve the signal/noise ratio of our reconstructions by combining the images before reconstruction. The poorer spatial resolution of the sum compromised the quality of the reconstructions, so we chose to reconstruct all the images individually. We then summed the 20 individually reconstructed images of each set and examined these two sums separately. The final reconstruction has 19 rows of 0.″44 extent each. Figure 1 illustrates the effects of reconstruction on our images.

We corrected our data for atmospheric and instrumental transmission by dividing by a spectrum extracted from the α Tau images and multiplying by a λ^{-2} Rayleigh-Jeans distribution fixed at 840 Jy at 8.7 μm. A photometrically calibrated infrared spectrum of α Tau has recently become available (Cohen, Walker, & Witteborn 1992). The spectrum shows deviations from a Rayleigh-Jeans distribution (of $\sim 15\%$ at 8 μm), but they will not affect our conclusions about relative changes in the spectra with spatial position.

3. ANALYSIS

Figure 2 presents the spectrum of the central row of the reconstruction of our better focused integration of HD 44179.

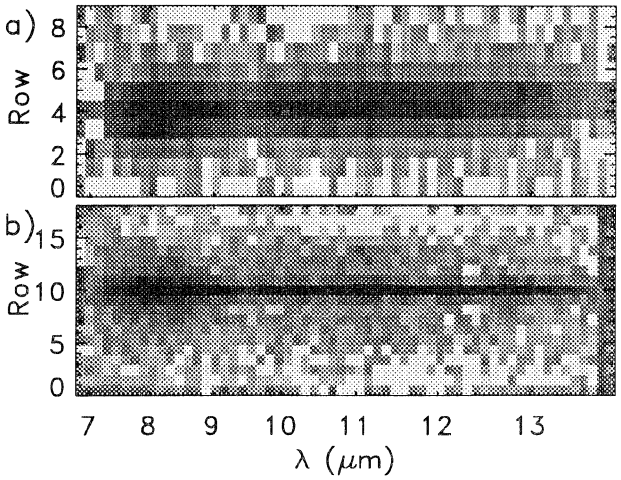

FIG. 1.—The results of MEMSYS maximum entropy reconstruction, illustrated by plotting the logarithm of the flux with gray-scale images. (*a*) A single HD 44179 image before reconstruction. (*b*) The sum of 20 reconstructed HD 44179 images from our second set of data. The reconstruction regridded the original 10 row data onto 19 rows and corrected for the angle between the dispersion axis and the array apparent in the top panel. The extended nature of the UIR features is evident in the reconstruction.

The UIR features are completely absent in the central row. Our reconstructions have resolved the UIR emission region and the central continuum source.

Despite the poorer focus of our first set of images of the Red Rectangle, we found that outside of the three central rows (9, 10, and 11), where the maximum entropy reconstruction algorithm had a difficult time disentangling UIR emission from continuum emission, the quality of both sets of reconstructions was similar. We produced Figure 3 by summing rows equidistant from the central continuum source on either side in groups of two. With the exception of rows 9 and 11 in the more poorly focused data set, we used all off-center rows from both reconstructions.

The side row spectra in Figure 3 contain very little of the continuum present in the central row; the features at 7.7, 8.6, 11.3, and 12.7 μm dominate the emission. These features show no obvious deviations from symmetry on either side of

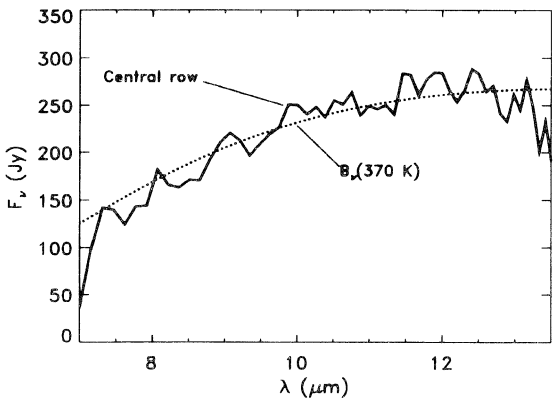

FIG. 2.—Comparison of the spectrum from the central row of our reconstruction of one set of HD 44179 images (*solid line*) with a 370 K blackbody (*dotted line*).

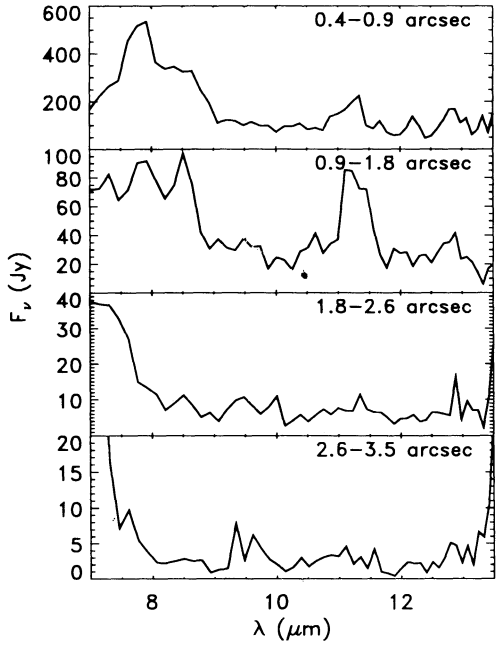

FIG. 3.—Spectra of emission from the Red Rectangle, moving from near HD 44179 (*top*) to the edge of the slit (*bottom*). Each spectrum is the sum of eight individual spectra: two adjacent rows on each side of the central source from both data sets. The exception is the top spectrum, which does not include the contribution from the rows adjacent to the central source in the set of images with the poorer focus.

HD 44179. They continue to the edge of the slit, where they disappear into the noise.

The character of the spectra changes dramatically with distance from HD 44179 (as illustrated in Fig. 3). The spectrum from the central region of the nebula (within 1″) dominates the emergent UIR flux and resembles very closely the nature of the UIR emission in all previously published spectra of the Red Rectangle. From 1″ to 2″ from the center, the strength of the 7.7 μm feature drops much more quickly than the strength of the 8.6 and 11.3 μm features and a second peak in the 7.7 μm feature becomes apparent at ~7.4 μm. Further from the center, this peak dominates the 7.9 μm flux, and the features at 8.6, 11.3, and 12.7 μm sink into the noise.

The rise in flux at 7.0 μm and 13.5 μm close to the edge of the slit may be attributable to the poor transmission at the edges of the 10 μm window. At the edges of the window, the difficulty in accurately determining the PSF as well as noise in the spectra of the Red Rectangle and α Tau all contribute to a low signal/noise ratio in the reconstructed spectra. For this reason, we doubt that the apparent feature at 7.0 μm is real.

To more carefully analyze the nature of the emission from the UIR features with position in the slit, we extracted the flux from each feature in each row of both our reconstructions. For a given feature, we held the wavelength interval over which we measured the flux fixed in all rows. We fitted the continuum to the data on either side of each feature. Separating the emission from the 7.7 and 8.6 μm features was not trivial. We first determined the total flux from the blended features, then fitted a linear "continuum" underneath the 8.6 μm feature running from the shoulder of the 7.7 μm feature at 8.0 μm to the continuum at 9.0 μm. The flux above this line we attributed to the 8.6 μm feature. By subtracting this from the total flux of the blended feature, we isolated the contribution of the 7.7 μm feature.

In Figure 4 we plot the flux of each feature against distance from HD 44179. Each point is a mean of four data: one from either side of the central source in each of the two reconstructions. We derived the error bars from the distribution of these four points. Because MEMSYS constrains the reconstructions to be positive, their statistics are decidedly non-Gaussian. This behavior means it would be incorrect to determine formal errors in the feature fluxes by traditional methods, such as using the root mean square of the deviations in the continuum. We have not included feature fluxes beyond four rows from HD 44179 in the reconstructions because we do not consider our measured fluxes beyond that point to be statistically meaningful.

The plots of three of the four feature fluxes, at 7.7, 8.6, and 12.7 μm, fall steadily from a maximum 0.″5 from HD 44179. The 11.3 μm feature behaves quite differently, initially dropping in strength, but then climbing to a secondary maximum 1.″4 (3 pixels) from the central source. This effect was seen on either side of HD 44179, in both sets of data. No such effect is seen in the other features.

4. DISCUSSION

4.1. *The Central Source*

The clean separation of the continuum source and the UIR features illustrated in Figure 2 allows us to examine the character of the spectrum of the central source without having to remove the effects of the UIR emission. The best fit to the central spectrum is a 370 K blackbody. Dainty et al. (1985) and Leinert & Haas (1989) have used speckle techniques in the near-infrared (from J to M) to resolve the central source of the Red Rectangle into a central component 0.″2 across and a larger component extended 0.″4 east/west and 0.″9 north/south. Based on the lack of polarization from the emission, Dainty et

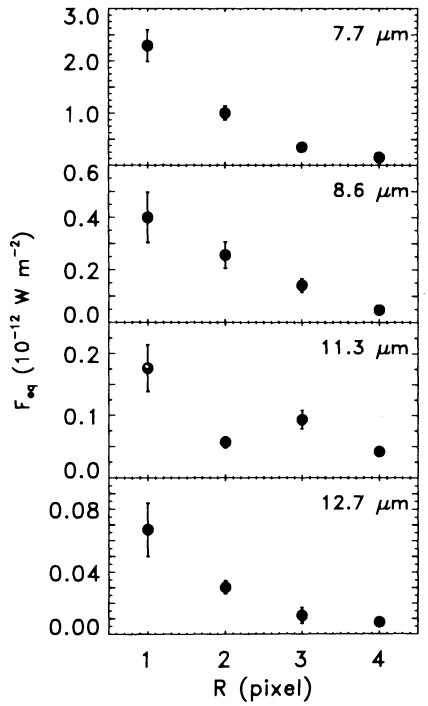

FIG. 4.—The flux of the four UIR features plotted against distance from the central source. One pixel is 0.″44 in the reconstructions.

al. attributed the flux to thermal radiation. We believe that the central continuum source we have observed corresponds to both the components seen at shorter wavelengths.

The lack of UIR emission in the central row of our reconstructions could be explained by a disk which is optically thick in the infrared. Given the geometry of the Red Rectangle, we would expect such a disk to be elongated east/west, in contradiction to the near-infrared speckle results. It is therefore more likely that there is a lack of carriers of the UIR features in the immediate vicinity of HD 44179. *We believe we have observed the formation of the carriers ~0".5 from HD 44179.*

4.2. *The 7.7 Micron Feature*

In the PAH model, several C—C stretching modes blend to form the 7.7 μm feature, while the 8.6 μm feature arises from a C—H bend in the plane of the aromatic ring. Sakata et al. (1987) were not able to obtain either feature in their QCC samples until they allowed them to oxidize; they explain the origin of these features as a cross-conjugated ketone. Blanco, Bussoletti, & Colangeli (1988) have not been able to produce the 7.7 and 8.6 μm features with their HAC model. They suggest that a mixture of hydrogenated amorphous carbon and PAHs may be necessary to fit the observed spectral characteristics. There is also a possibility that various molecular groups originally invoked by Duley & Williams (1981) may contribute to the nature of the emission in this wavelength regime.

Differences in the peak wavelength and relative shape of the 7.7 μm feature have been emphasized by Cohen et al. (1989) and Bregman (1989). They have noticed that the peak wavelength of this feature is closer to 7.8 μm in planetary nebulae while in reflection nebulae and H II regions, the peak occurs at shorter wavelengths, 7.7 and 7.6 μm, respectively. High spectroscopic resolution observations of NGC 7027 by Bregman et al. (1986) explain this shift by showing that the 7.7 μm feature is actually a combination of two features, at ~7.8 and 7.6 μm. The peak wavelength depends on the relative intensities of the two blended features.

We believe that for the first time, the peak wavelength of the 7.7 μm feature has been observed to shift with spatial position within an object. In the Red Rectangle, the feature appears to have two components, one at 7.9 and the other at ~7.4 μm. As the distance from HD 44179 increases, the intensity of the 7.9 μm feature decreases with respect to the intensity of the 7.4 μm feature, resulting in a shift of the peak wavelength of the blend to shorter wavelengths. Because of the poor atmospheric transmission shortward of 8 μm, the signal-to-noise ratio is lower here than at longer wavelengths and raises the concern that the apparent wavelength shift may not be real. We have tested our reconstruction method and do not believe that this effect is an artifact of our algorithm. Nonetheless, we suggest that this result be treated cautiously until it is independently confirmed.

We can rule out the possibility that the emission at 7.4 μm is due to the Pfund α recombination line of hydrogen. Thronson (1982) gives an upper limit (2 σ) to the flux from the Brackett γ line of 1.5×10^{-15} W m^{-2}. Assuming a temperature of 10^4 K and a density of 10^4 cm^{-3}, and taking into account the difference in extinction between 2.2 and 7.4 μm, the upper limit to the flux from Pfund α would be 8.5×10^{-15} W m^{-2}, ~5% of the flux actually measured. Estimates based on the radio free-free upper limits reported in Cohen et al. (1975) produce upper limits to the Pfund α emission which are smaller by at least a factor of 50.

The PAH model ascribes the 7.7 μm feature to a blend of C—C stretches, so a shift in peak wavelength with distance from HD 44179 could indicate changes in composition of the dust or in the physical conditions of the nebula. Given the uncertain nature of the specific components of the 7.7 μm feature in the different models of the UIR features, it is difficult to relate the shift in peak wavelength at 7.7 μm to any specific mechanism.

4.3. *8.6, 11.3, and 12.7 Micron Features*

The UIR emission appears to arise from two spatially distinct zones. The 7.7 μm feature dominates in the inner zone, within 1" of the central source, while emission from the UIR features at 11.3 and 8.6 μm becomes much more significant 1"–2" away. If the 7.7 μm feature truly arises from a C—C stretch and the other features from C—H bends, this dichotomy may indicate the degree of dehydrogenation close to the central source.

All the proposed carriers of the UIR emission will produce the 11.3 μm feature from an out-of-plane bend of a C—H bond on the periphery of an aromatic ring. The precise wavelength of the feature depends on the number of adjacent H atoms on the same ring. If the H atom is isolated (solo mode), the feature appears at 11.3 μm. If the bend occurs in an H atom with a single neighbor (duo mode), the transition is seen at ~11.9 μm, while the trio mode (two neighbors) radiates at ~12.7 μm. Studies of IRAS Low-Resolution Spectrometer data by Cohen, Tielens, & Allamandola (1985) and higher resolution spectroscopy by Witteborn et al. (1989) support this model. They found that a feature at 12.7 μm frequently accompanies the 11.3 μm feature, although the 11.9 μm emission is usually weak or nonexistent, possibly because it is smeared into the emission plateau which runs from 11 to 13 μm. They argue that the low excitation of some of their sources rules out the possibility that the 12.7 μm flux actually arises from the [Ne II] emission line at 12.78 μm, and we will assume this to be the case in our discussion below. High-resolution spectroscopy would settle this issue.

The sharp increase of emission at 11.3 μm compared to the emission at 12.7 μm at ~1.5" from HD 44179 indicates that the solo mode dominates at this distance. This effect could result from a favorable grain geometry or because the molecules or grains are partially dehydrogenated. Higher levels of hydrogenation further from HD 44179 could explain why this enhancement does not persist with increasing distance.

4.4. *Nature of the Red Rectangle*

Leinert and Haas emphasize that the current model of the Red Rectangle has problems. At a distance of 330 pc (Cohen et al. 1975), the energy output from the Red Rectangle corresponds to 920 $L_\odot$ while the luminosity from a B9-A0 III star could be at most 240 $L_\odot$. Rowan-Robinson & Harris (1983) attempted to resolve this difficulty by suggesting that either the object was much closer than 330 pc or that the power output was driven by a second, obscured star. Leinert & Haas were led to conclude that the second possibility was the best explanation. While it is plausible, it invokes two rare occurrences: a hidden component buried by many magnitudes of extinction and an object with the rare spectral type B9-A0 III.

We propose that it is possible to explain the Red Rectangle with a simpler model, that of an accretion disk around a degen-

erate star. An accretion disk would naturally produce a bipolar outflow morphology. In addition, the broad, flat spectral energy distribution (Leinert & Haas 1989, their Fig. 11) is very suggestive of emission from an accretion disk. The central object must be degenerate because a larger object could not produce the observed luminosity without an unreasonably large mass infall rate.

In this scenario, the 10^4 K blackbody and the B9-A0 III spectrum could both arise from radiation from the inner, gaseous portions of the accretion disk. This model would explain several unusual characteristics of the spectrum of HD 44179. Greenstein & Oke (1977) were unable to fit any B type model atmosphere to its large Balmer jump. They further pointed out the inconsistency of a spectral class of late B with the appearance of the O I and C I absorption lines reported by Cohen et al. (1975). The bizarre ultraviolet spectrum of HD 44179, with its emission and absorption features of CO and related carbon molecules (Sitko 1983) represents yet another inconsistency with a classification of late B. Accretion disk models naturally produce a variety of spectral features which cannot be reconciled with a single spectral type.

The tremendous velocity widths observed by Sitko (1983) of 1000 km s^{-1} imply that the escape velocity from the central object must be much larger than that appropriate to a normal late B giant. Furthermore, the H and K absorption lines observed by Cohen et al. (1975) are redshifted with respect to the star by 30 km s^{-1}, suggesting infall in the line of sight toward HD 44179. These kinematic features fit easily into our picture of an accretion disk around a degenerate object.

5. SUMMARY

For several reasons, we believe we have observed the evolution of the particles responsible for the UIR emission features in the outflow from HD 44179. There is no UIR emission in the immediate vicinity of the central continuum source, suggesting that the UIR carriers have not yet formed this close to the outflow source. The peak wavelength of the 7.7 μm feature appears to shift to shorter wavelengths further from HD 44179, indicating a change in the nature of the emitting material. The drop in relative significance of the 7.7 μm feature from 1″ to 2″ from HD 44179 suggests the material may be growing increasingly hydrogenated as it evolves. This idea is further strengthened by the enhancement of the 11.3 μm feature at these distances and its decline in strength relative to the 8.6 and 12.7 μm features further away.

A model of HD 44179 as an accretion disk around a degenerate object would eliminate many difficulties with present models and explain all of the observed properties of the Red Rectangle in terms of one simple model.

We are grateful to R. Canterna for providing the computer facilities on which we analyzed our data. H. M. Dyck made many valuable comments on the manuscript. Astronomy at WIRO is supported by the State of Wyoming and the Air Force Office of Scientific Research.

REFERENCES

Allamandola, L. J., Tielens, A. G. G. M., & Barker, J. R. 1985, ApJ, 290, L25
———. 1989, ApJS, 71, 773
Blanco, A., Bussoletti, E., & Colangeli, L. 1988, ApJ, 334, 875
Bregman, J. D. 1989, in Interstellar Dust, ed. L. J. Allamandola & A. G. G. M. Tielens (Dordrecht: Kluwer), 109
Bregman, J. D., Allamandola, L. J., Tielens, A. G. G. M., Witteborn, F. C., Rank, D. M., & Wooden, D. 1986, in Proc. Summer School on Interstellar Processes: Abstracts of Contributed Papers (Moffett Field, CA: NASA), 117
Cohen, M., et al. 1975, ApJ, 196, 179
Cohen, M., Allamandola, L., Tielens, A. G. G. M., Bregman, J., Simpson, J. P., Witteborn, F. C., Wooden, D., & Rank, D. 1986, ApJ, 302, 737
Cohen, M., Tielens, A. G. G. M., & Allamandola, L. J. 1985, ApJ, 299, L93
Cohen, M., Tielens, A. G. G. M., Bregman, J., Witteborn, F. C., Rank, D. M., Allamandola, L. J., Wooden, D. H., & de Muizon, M. 1989, ApJ, 341, 246
Cohen, M., Walker, R. G., & Witteborn, F. C. 1992, AJ, 104, 2030
Dainty, J. C., Pipher, J. L., Lacasse, M. G., & Ridgway, S. T. 1985, ApJ, 293, 530
Duley, W. W., & Williams, D. A. 1981, MNRAS, 196, 269
Geballe, T. R., Tielens, A. G. G. M., Allamandola, L. J., Moorhouse, A., & Brand, P. W. J. L. 1989, ApJ, 341, 278
Gillett, F. J., Forrest, W. J., & Merrill, K. M. 1973, ApJ, 183, 87
Grasdalen, G. L., Sloan, G. C., & LeVan, P. D. 1992, ApJ, 384, L25 (Paper I)
Greenstein, J. C., & Oke, J. B. 1977, PASP, 89, 131
Gull, S. F., & Skilling, J. 1984, I.E.E. Proc. 131, 646
——. 1989, Quantified Maximum Entropy "MEMSYS 3" Users' Manual (London: Maximum Entropy Data Consultants Ltd.)
Jones, A. P., Duley, W. W., & Williams, D. A. 1990, QJRAS, 31, 567
Landau, R., Grasdalen, G., & Sloan, G. C. 1992, A&A, 259, 696
Léger, A., d'Hendecourt, L., & Défourneau, D. 1989, A&A, 216, 148
Léger, A., & Puget, J. L. 1984, A&A, 137, L5
Leinert, Ch., & Haas, M. 1989, A&A, 221, 110
LeVan, P. D. 1990, PASP, 102, 190
Rowan-Robinson, M., & Harris, S. 1983, MNRAS, 202, 767
Sakata, A., Wada, S., Onaka, T., & Tokunaga, A. T. 1987, ApJ, 320, L63
———. 1990, ApJ, 353, 543
Sakata, A., Wada, S., Tanabé, T., & Onaka, T. 1984, ApJ, 287, L51
Sellgren, K. 1984, ApJ, 277, 623
Sitko, M. L. 1983, ApJ, 265, 848
Sloan, G. C., Grasdalen, G. L., & LeVan, P. D. 1993, ApJ, 404, 328 (Paper II)
Thronson, H. 1982, AJ, 87, 1207
Walker, R., & Price, S. D. 1975, AFCRL Infrared Sky Survey, AFCRL-TR-75-0373
Witteborn, F. C., Sandford, S. A., Bregman, J. D., Allamandola, L. J., Cohen, M., Wooden, D. H., & Graps, A. L. 1989, ApJ, 341, 270
Zuckerman, B., Gilra, D. P., Turner, B. E., Morris, M., & Palmer, P. 1976, ApJ, 205, L15